17th World Conference on Earthquake Engineering, 17WCEE
Sendai, Japan - September 13th to 18th 2020

EXPERIMENTAL STUDY OF A NOVEL ASYMMETRIC NONLINEAR MASS DAMPER FOR SEISMIC RESPONSE MITIGATION

J. Wang[(1)], Y. Zheng[(2)], B. Wang[(3)], Z. Liu[(4)] , C. Zhang[(5)], H. Li[(6)]

[(1)] *Assistant professor, School of Civil Engineering, Guangzhou University, wangjj@gzhu.edu.cn*
[(2)] *Engineer, China Construction Fourth Engineering Division Corp. Ltd., zheng_yuqiang@cscec.com*
[(3)] *Post-doctoral researcher, Department of Architecture and Architectural Engineering, Kyoto University, cebinwang@gmail.com*
[(4)] *Graduate student, Key Laboratory of Earthquake Resistance, Earthquake Mitigation and Structural Safety, Ministry of Education, Guangzhou University, 1111916007@e.gzhu.edu.cn*
[(5)] *Graduate student, School of Civil Engineering, Hunan University of Technology, zhangchao4933342@yeah.net*
[(6)] *Graduate student, School of Civil Engineering, Hunan University of Technology, lihaobo521@yeah.net*

Abstract

Structural control technologies, especially passive ones, have been developed as effective measures to mitigate undesired response of civil structures in the past decades. Tuned mass dampers (TMDs) are one of the most applied passive control technologies. The high control performance of TMDs is obtained by tuning the frequency of TMDs to the frequency of primary structures for resonant motions. This frequency tuning, however, posts potential risk of ill performance when the frequency of primary structure shifts from its initial designs. By contrast, nonlinear energy sinks (NESs), with a nonlinear force-displacement relationship, are competent to reduce structural responses within a wide range of frequencies. Since the dynamics of a NES is relevant to its relative motions to the primary structure, the nonlinearity of NESs also makes the effectiveness of NESs depend on the input energy level. To address these issues, a novel passive mass damper, namely asymmetric nonlinear energy sink (Asym NES), is proposed in this study. Asym NESs, configured based on conventional NESs, are characterized by integrating linear and nonlinear restoring forces to mitigate the unwanted responses of building structures. In particular, Asym NESs consist of an auxiliary mass which is statically balanced at a deformed position through a linear and a nonlinear spring. This configuration produces an asymmetric restoring force in the Asym NES. First, the restoring force of Asym NESs and the equations of motion of an Asym NES-attached structural system are derived. Subsequently, the Asym NES is experimentally tested on a small-scale three-story steel frame the natural frequencies of which can be altered by changing the number of columns per story. The performance of the Asym NES is also compared with a TMD and a cubic NES under impulsive excitations. Test results demonstrate the effectiveness of the Asym NES as well as its robustness against changes in the structural frequency. The validated Asym NES model is further applied in the numerical investigation on a six-story benchmark building to highlight its effectiveness and robustness in potential practical applications. A suite of 106 seismic ground motions with wide-ranged energies are applied to the structures with original and decreased frequencies. The results show that the Asym NES processes high effectiveness in response reduction and strong robustness against changes in both structural frequency and input energy level, exhibiting great potential in response control under extreme seismic events.

Keywords: structural control, passive control, nonlinear energy sink, energy robustness, seismic response

1. Introduction

Structural control technologies have been developed as effective measures to mitigate undesired responses of buildings, bridges, and infrastructures in the past decades [1]. Although active and semi-active control approaches have witnessed great progress and provided higher control capacity than their passive counterparts [2-4], passive structural control technologies are still much more widely applied in engineering practice nowadays. The advantages of passive control strategies lie in their stability, reliability, and simplicity without any need for power supply and feedback system. Tuned mass dampers (TMDs) are one of the most widely used structural control devices in practical applications currently [5]. A TMD consists of a secondary mass connected to the primary system through a linear spring and a damper. By resonating out of phase with the primary structure, the TMD transfers a considerable amount of energy from the primary structure to the auxiliary mass and eventually damps out the transferred energy with large relative motions. From the design point of view, TMDs do not interfere with vertical and horizontal load paths and are therefore relatively easy to implement in new buildings and in existing ones [6].

To ensure an effective control performance of TMDs, the key point is to select proper mass, stiffness, and damping for the TMD. The tuning approaches that determine the relationship between the natural frequencies of the TMD and the primary structure have, therefore, become a subject of interest in TMD studies. To date, TMDs have been extensively adopted to enhance the serviceability of tall buildings under wind loadings [7-9]. Meanwhile, researchers also extended it into the community of earthquake engineering in the past years. Some optimum TMD parameters and optimization algorithms have been derived under various types of ground excitations [10-12], part of which considered the uncertainties resulted from the changing environment [13-15]. However, the seismic response mitigation effect of conventional TMDs had not been effective as the TMD had little effect on the maximum responses under earthquakes [16]. Additionally, a considerable mass of TMD was required to achieve a sizeable reduction in the response, especially for structures with large damping ratios [6], which in turn compromised the applicability of TMDs. More importantly, the most challenging issue of the TMD is that its effectiveness can be drastically undermined when the TMD is detuned [17] or when the system exhibits nonlinear behavior [18] which is likely to happen to structures under extreme seismic events.

In contrast to TMDs that are featured by linear force–displacement relationships, nonlinear energy sinks (NESs) are a type of passive energy absorbers which possess essentially nonlinear (i.e., a non-linearizable restoring force). This nonlinearity enables NESs to effectively reduce the structural responses over a wide range of frequencies and to transfer energy from the primary structure to the device in a one-way irreversible manner (known as targeted energy transfer) [19,20]. NESs can also excite the higher vibration modes of the primary structure where the energy is dissipated more rapidly [21-23]. Both experimental and numerical studies have been carried out to demonstrate the robustness of NESs against changes in the natural frequency of primary structures [24-29]. The frequency-robustness of NESs results from the continuous change of the stiffness at different displacements. This changing stiffness enables the NESs to vibrate at different frequencies. It is obvious that the frequency range of an NES must contain the fundamental vibrational frequency of the primary structure to ensure the occurrence of resonance for an effective response reduction. However, for the most studied NESs that have cubic force–displacement relationships, the control efficiency may deteriorate when the input energy is not optimal [30]. Not only the control performance is degraded due to the discrepancy between the frequencies of the cubic NES and the primary structure but also damages may be caused by the larger force to local structural components. To address this issue, mass dampers with both linear and nonlinear characteristics have been developed, which allows the control device to be robust against changes in both the energy level and the structural frequency [31,32].

In this paper, a novel passive mass damper, namely asymmetric NES (Asym NES) is developed. The proposed Asym NESs aim to reduce the unwanted energy dependence while keeping the favorable frequency robustness of conventional NESs. Asyms NES are configured based on cubic NESs and have two types of springs including a cubic spring and a linear spring. The restoring force of the Asym NES and the equations of motion (EOMs) of an Asym NES-attached structural system are derived. The Asym NES is

experimentally tested on a small-scale three-story steel frame structure with different column layouts. In the experiment, a comparable TMD and cubic NES are also realized and the measured responses of these control systems are analyzed. The Asym NES is investigated numerically on a six-story moment-resisting-frame (MRF) structure with different structural frequencies. The control performance of the Asym NES is further examined when subjected to a suite of 106 seismic ground motions with various input energies.

2. Asymmetric nonlinear energy sink

An Asym NES consists of an auxiliary mass attached to the primary structure through two types of springs including a cubic-type nonlinear spring and a linear spring. The cubic spring is realized through the same configuration as employed in the cubic NES (Fig.1(a)), where the attached mass is connected to the primary structure through springs perpendicular to its moving direction. The perpendicular springs are unstressed at the undeformed position. The force in the moving direction of the mass resulting from the perpendicular springs is given by Eq. (1).

$$f = 2k\left(\sqrt{l^2 + x^2} - l\right)\left(x/\sqrt{l^2 + x^2}\right) = \left(k/l^2\right)x^3 + \mathrm{o}\left(x^3\right) \tag{1}$$

where k is the stiffness of the springs, l is the original length of the springs, and x is the displacement of the mass m from the undeformed position. This force can be rewritten in Taylor's Expansion so that when the displacement is relatively small, the higher order terms can be neglected. The force therefore can be written as in Eq. (2).

$$f = k_{\mathrm{Cubic}}x^3 \tag{2}$$

where $k_{\mathrm{Cubic}} = k/l^2$.

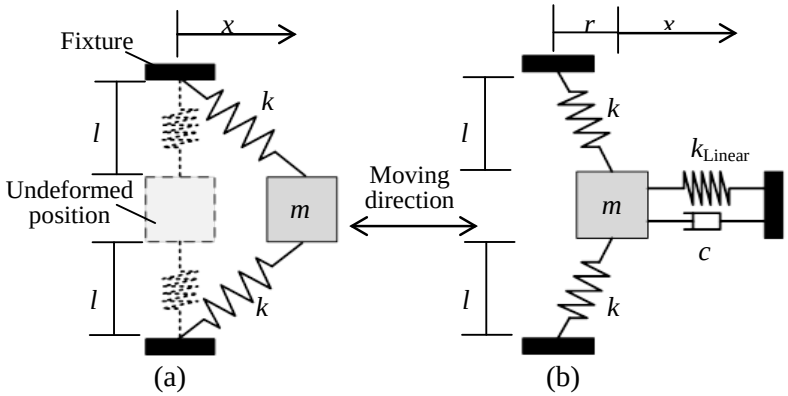

Fig. 1 – Conceptual models of (a) cubic NES and (b) Asym NES

The Asym NES (Fig.1(b)) introduces a linear stiffness element into the cubic NES. The mass reaches static equilibrium at a deformed position. The cubic force is balanced with the linear force produced by the linear spring. Taking the static balanced position as the initial position, the cubic and linear forces in the moving direction of the mass are shown in Eqs. (3) and (4), respectively.

$$f_{\mathrm{Cubic}}\left(x\right) = k_{\mathrm{Cubic}}\left(x + r\right)^3 \tag{3}$$

$$f_{\mathrm{Linear}}\left(x\right) = k_{\mathrm{Linear}}x + f_0 \tag{4}$$

where r is the distance between the undeformed position and the static balanced position, k_{Linear} is the stiffness of the linear spring, and f_0 is the initial linear force in the linear spring at the statically balanced

position. This initial force can be obtained by solving the force equation at the statically balanced position as shown in Eqs. (5) and (6).

$$f_{\text{Cubic}}(0) = f_{\text{Linear}}(0) \tag{5}$$

$$f_0 = -k_{\text{Cubic}} r^3 \tag{6}$$

Therefore, the resultant spring force of the Asym NES becomes

$$f_{\text{Spring}} = k_{\text{Cubic}}(x+r)^3 + k_{\text{Linear}} x - k_{\text{Cubic}} r^3 \tag{7}$$

The damping force of the Asym NES is

$$f_{\text{Damping}} = c\dot{x} \tag{8}$$

where c is the damping coefficient of the device.

Fig.2 compares the spring force–displacement relationships of a TMD, a cubic NES, and an Asym NES. Fig. 2(c) shows the linear and cubic spring force components of the Asym NES. The nonlinearity is of a less degree in the Asym NES than in the cubic NES in either the positive or the negative direction, but the overall adjustability to the tuning of frequency is enhanced due to the asymmetric force–displacement relationship observed in the Asym NES.

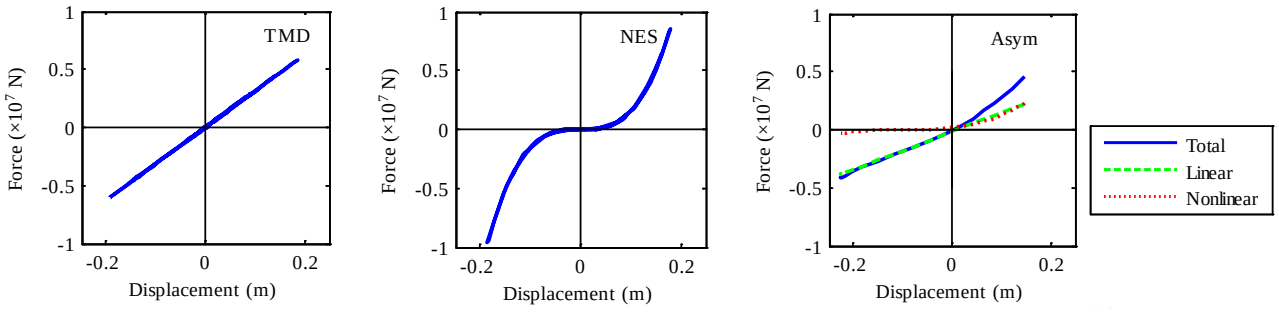

(a) (b) (c)

Fig. 2 – Force–displacement relationships: (a) TMD, (b) cubic NES, and (c) Asym NES

3. Experimental study

3.1 Primary structure and equations of motion

In this section, the Asym NES was experimentally tested on a small-scale three-story steel frame structure. The structure consisted of three identical floor plates and a base plate. The floor plates with a dimension of 440 mm×440 mm×15 mm were connected with the columns by steel bolts. A smaller steel plate with a dimension of 300 mm×300 mm×10 mm was designed as an additional weight for every story. This smaller plate can be removed to install the fixtures and the control devices in the top story so that the total weight of each story would be kept approximately the same. The base plate had a dimension of 1100 mm×1100 mm×15 mm and can be regarded as a rigid foundation for the test structure. The columns were made from mangalloy (i.e., manganese steel) to ensure large displacement capacity without yielding. With this feature, the structure can be assumed to be elastic. The effective heights of the columns at the first (bottom) story, the second story, and the third (top) story were 225 mm, 235 mm, and 235 mm, respectively. The columns had a cross-section of 80 mm×1.5 mm with the distinctive strong and weak axes so that the structure can only move along the weak axis of the column section. The geometric configuration and physical setup of the test

frame are given in Fig.3. To investigate the sensitivity of the proposed control strategy to the variable property of the primary structure, two different column layouts were considered in the experiment. The structure with six columns on every story was deemed as the intact primary structure while the structure with four columns on every story represented the damaged primary structure. The Asym NES that was designed for the six-column structure will be tested on both structures.

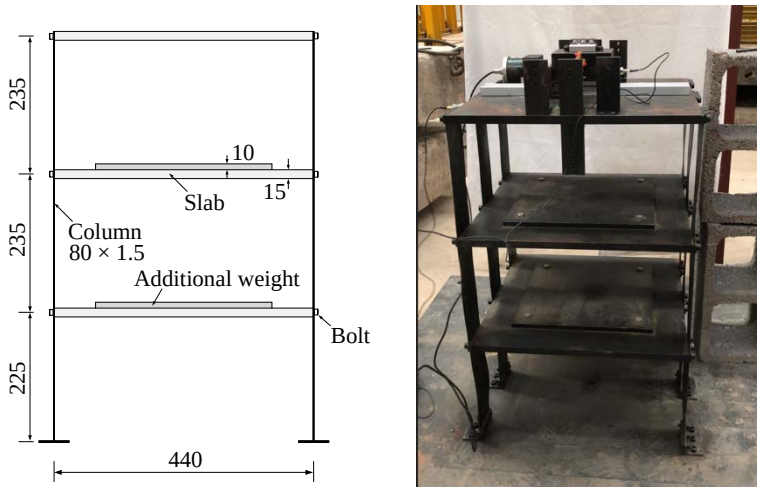

Fig. 3 – Geometric configuration and physical setup of the test frame (unit: mm)

System identification was performed on the six-column and four-column structures without any control devices functioning on the top story. In these uncontrolled structures, the upper plate of the top story was replaced by the fixtures of the control device. An additional mass block of 4.58 kg which was the mass of the Asym NES was also fastened to the top story. The resulted floor masses were 32.40 kg for the top story and 29.61 kg for the middle and bottom stories. The ICP-type accelerometers (Model 601D manufactured by AFT Electronic Technology Co., Ltd.) were used to measure the story accelerations. The data acquisition system AZ804-A and analyzer AZ308 (manufactured by CRAS Co., Ltd.) were used with a sampling rate of 1000 Hz throughout the experiment. The displacements were obtained by integrating the measured accelerations over time twice and a bandpass filter from 1 Hz to 20 Hz was applied to the experimental data. The identified natural frequencies of the six-column primary structures were 2.02 Hz, 5.75 Hz, and 8.25 Hz for the first, the second, and the third modes, respectively, whereas the natural frequencies of the four-column primary structure were 1.57 Hz, 4.51 Hz, and 6.49 Hz for the first, the second, and the third modes, respectively. A fundamental modal damping ratio of 0.3% was identified for both structures.

The Asym NES is attached to the top story of the primary structure so that the auxiliary mass will experience the strongest motion possible. The EOM for the Asym NES is

$$m_{\mathrm{A}}\ddot{x}_{\mathrm{A}} + f_{\mathrm{Spirng}} + f_{\mathrm{Damping}} = -m_{\mathrm{A}}\left(\ddot{x}_3 + \ddot{x}_{\mathrm{g}}\right) \tag{9}$$

where x_3 is the displacement of the top story relative to the ground, $\ddot{x}_{\mathrm{g}}$ is the ground acceleration, x_{A} is the displacement of the Asym NES relative to the top story of the primary structure, m_{A} is the mass of the Asym NES, and f_{Spring} and f_{Damping} is the restoring force and the damping force of the Asym NES as defined in Eqs. (7) and (8), respectively.

For the primary structure, the spring force and damping force produced by the Asym NES can be seen as external forces exerted on the top mass. Therefore, the EOMs for the primary structure written in matrix form are

$$\mathbf{M}\ddot{\mathbf{x}} + \mathbf{C}\dot{\mathbf{x}} + \mathbf{K}\mathbf{x} = \mathbf{G}\begin{Bmatrix} \ddot{x}_{\mathrm{g}} \\ f_{\mathrm{Spirng}} + f_{\mathrm{Damping}} \end{Bmatrix} \tag{10}$$

$$\mathbf{x} = \{x_1 \quad x_2 \quad x_3\}^{\mathrm{T}} \tag{11}$$

$$\mathbf{G} = \begin{Bmatrix} -m_1 & -m_2 & -m_3 \\ 0 & 0 & 1 \end{Bmatrix}^{\mathrm{T}} \tag{12}$$

where m_i is the mass of the i^{th} story of the primary structure, x_i is the displacement of the i^{th} story relative to the ground, **M**, **C**, and **K** are the mass, damping, stiffness matrices of the primary structure, respectively, and **G** is the influence matrix for loadings.

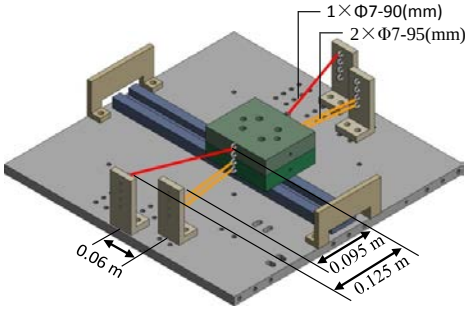

Fig. 4 – Experimental configuration of the Asym NES

Table 1 – Identified parameters of three devices

Device	Stiffness coefficient		Viscous damping coefficient (N·s/m)		Friction coefficient
	Linear (N/m)	Cubic (N/m^3)	Six-column	Four-column	
Asym	200	9.5×10^4	2.3	3.8	0.003
TMD	780	—	2.5	3.8	0.003
NES	—	4.8×10^5	2.3	2.3	0.003

3.2 Design of Asym NES and model validation

The Asym NES had a mass that was 5% (4.58 kg) of the total mass of the structure. To investigate this novel control device, the Asym NES was physically compared with a TMD and a cubic NES with the same mass ratio. The auxiliary mass moved along a sliding rail through a series of bearings. Baffles were placed at both ends of the rail as a safety measure. Both the linear and the cubic springs were realized by sets of rubber cords with a diameter of 7 mm, which connected the auxiliary mass to the fixtures in the transverse direction. The set of pre-tensioned rubber cords represented the linear spring in the TMD, whereas the set of unstretched rubber cords represented the cubic spring in the cubic NES. For the Asym NES (Fig.4), two sets of rubber cords connected to different pairs of fixtures were used, representing the linear spring and the cubic spring. The design parameters of the Asym NES were determined based on the identified model of the six-column primary structure. Numerical optimization was carried out in the MATLAB [33] to obtain the linear and nonlinear stiffnesses of the Asym NES. An initial velocity of 0.2 m/s was applied to every mass in the system. The objective of the optimization was to minimize the root-mean-square (RMS) of the top story displacement of the six-column primary structure during the initial 10 s (approximately 20 cycles). The comparable TMD and cubic NES were optimized by the same objective as the Asym NES. The actual parameters of the devices were, however, somewhat different from the design values due to the manufacture

discrepancies. The resulting parameters for the Asym NES, the TMD, and the cubic NES are listed in Table 1.

To validate the analytical and numerical models of the Asym NES-attached structural system, the experimental responses of the Asym NES structure under free vibrations were compared with its numerical counterparts. Fig.5 shows the displacements of the auxiliary mass and the top story of the Asym NES structure with four columns as an example. The numerical predictions agreed well with the experimental responses generally.

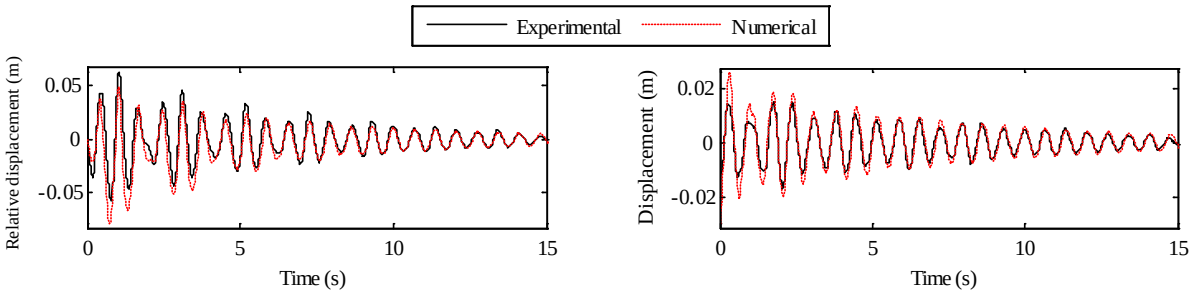

(a) (b)

Fig. 5 – Experimental and numerical responses of the Asym NES structure: (a) device displacement and (b) top story displacement

3.3 Response investigation and discussions

In the experiment, the Asym NES structure, the TMD structure, the cubic NES structure, and the uncontrolled structure were considered. All structures were subjected to the same initial-displacement condition. The top story was forced statically to have a 0.03 m deformation relative to the base plate and no external force was imparted to the middle and bottom stories. The initial displacements of the middle and bottom stories can be calculated using the identified stiffness distributions of the primary structures.

Fig.6 illustrates the displacements of the top story for all the structures considered. As these control devices were designed for the six-column primary structure, all three control strategies were very effective in reducing the responses of the intact structure. Slight beating phenomenon was observed in the controlled responses due to the very small damping of the experimental setup. This beating phenomenon was the most observant in the TMD structure because that an in-tune TMD adds a new frequency to the system which is very close to the fundamental frequency of the primary structure. The Asym NES was capable of attenuating the responses as effectively as the TMD and the cubic NES. For the four-column structures, the fundamental natural frequency of the uncontrolled structure decreased from 2.02 Hz to 1.57 Hz, representing the property change from an intact structure to a damaged structure. The TMD deteriorated in response mitigation as it was no longer in tune with the primary structure. On the contrary, the cubic NES and the Asym NES maintained a relatively good performance compared to the TMD, although the two devices were not specifically designed for the four-column primary structure. From the above discussion, the Asym NES demonstrated both the linear and nonlinear dynamic characteristics as an integrated control strategy with favorable control effectiveness and strong frequency robustness.

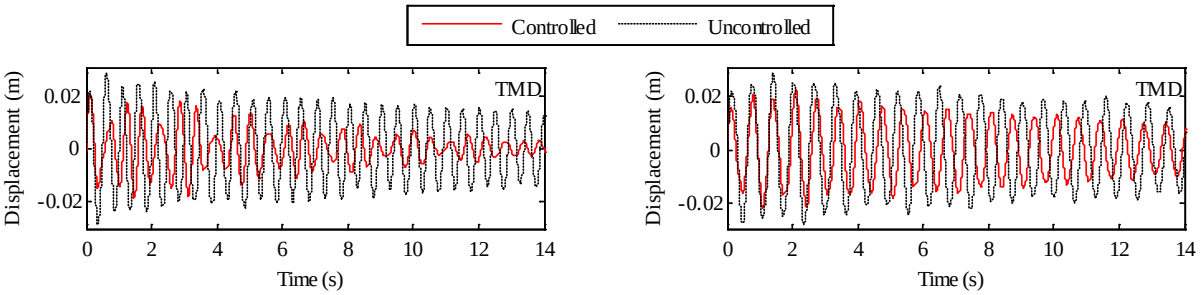

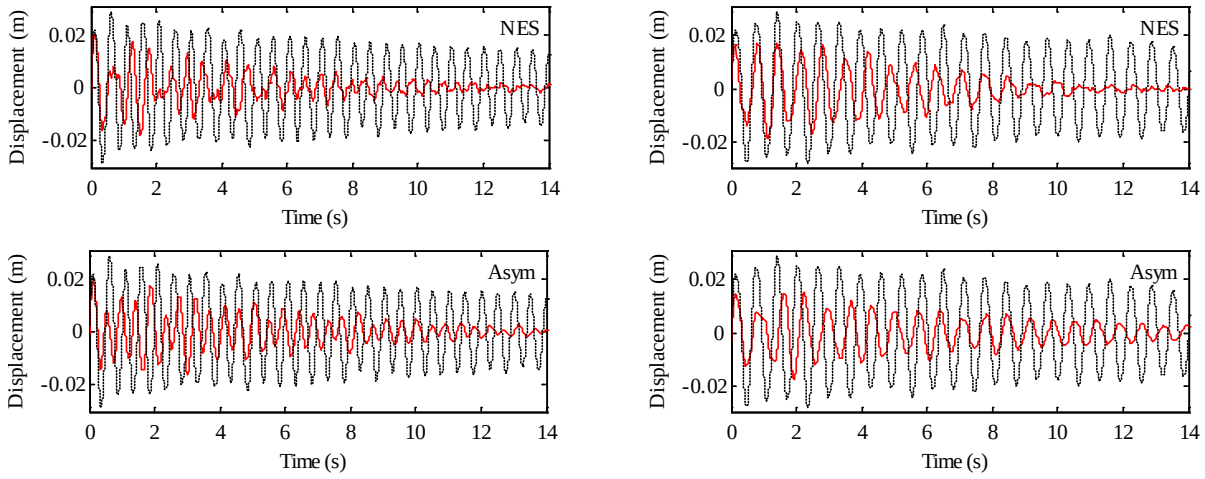

(a) (b)

Fig. 6 – Experimental responses of (a) six-column structures and (b) four-column structure

4. Seismic application

4.1 Optimization of Asym NES on a six-story primary structure

The control capacity of the Asym NES was numerically investigated on a six-story steel MRF structure illustrated in the FEMA P-751 [34]. The special steel MRFs on the perimeter of the building provide the lateral load resistance for the structure. The building is designed as an office building which consists of five bays at 8.53 m in the north-south (N-S) direction and six bays at 9.14 m in the east-west (E-W) direction. This MRF structure was condensed into a linear lumped-mass model moving only in the N-S direction. The model assumes Rayleigh damping with a 2% damping ratio for the first and the third modes. The fundamental natural period of the primary structure is 0.62 s.

The three control devices were considered and separately attached to the top story of the primary structure. To compare the control capacity of the devices (especially the portion contributed by their springs), parameters including the mass and the damping were set the same values for all the three types of mass dampers. Considering the space limitation in the practical application, a mass of 3.95×10^5 kg that was 5% of the total mass of the primary structure was employed. The optimizations were conducted under an impulsive excitation which was exerted to the structure by applying an initial velocity of 0.8 m/s to every mass in the system. The objective was to minimize the RMS of the top story displacement during the initial 10 s. The global search algorithm was applied for the optimization. The stiffness and the damping coefficients of the TMD were optimized to be 3.13×107 N/m and 1.08×106 N·s/m, respectively, corresponding to a frequency ratio to the primary structure of 0.88 and a damping ratio of 15.41%. This damping was then used for the cubic NES and the Asym NES. For the cubic NES, the optimized nonlinear stiffness coefficient was 1.50×109 N/m^3. For the Asym NES, a deformed distance of 0.2 m was preset which was deemed reasonable in consideration of the stroke. The optimal linear and nonlinear stiffness coefficients were 1.41×108 N/m and 7.33×107 N/m^3, respectively.

4.2 Seismic response investigation

The seismic performance of the Asym NES was evaluated under a suite of 106 ground motions from the Imperial Valley earthquakes happened during the period from 1938 to 1979. These seismic records were downloaded from PEER Ground Motion Database [35]. Information including earthquake name, year, magnitude, station name, file name and peak ground acceleration (PGA) can be found in [32]. The PGAs of these records were wide-ranged from 0.065 m/s^2 to 7.614 m/s^2, representing earthquakes of various energy levels. The power spectral densities of these earthquakes were not limited to any specific types.

The seismic excitations were applied to the four systems with the original structural frequency and the decreased structural frequency (75% of the original value), respectively. Figs.7 and 8 compare the RMS top story displacements of the original-frequency structures and the decreased-frequency structures under the earthquakes, respectively. In these figures, the sequences of the earthquakes in the abscissa were rearranged in the increasing order of the uncontrolled responses (solid black lines in the figures). Although the frequency characteristics of earthquakes will affect the performance of control devices, their relationship was not the focus of this study and therefore was not discussed herein. In a sense, the TMD can be seen as the standard control method as a well-tuned TMD can effectively dissipate energy through its resonance with the primary structure. In Fig.7, the TMD structure had the smallest responses among all the systems with original frequency under the majority of the earthquakes. However, the performance of the TMD deteriorated greatly in Fig.8 as it became detuned when the structural frequency decreased. The performance of the cubic NES was very sensitive to the input energy level and was understandably less effective than the TMD and the Asym NES for original-frueqency structures. When the structural stiffness decreased, the structual responses were generally larger and shifted closer to the optimal response level of the cubic NES. Consequently, the cubic NES performed better on the decreased-frequency structure than on the original-frequency structure. The Asym NES was almost as effective as the in-tune TMD for the structure with original frequency regardless of the energy levels of the earthquakes. When the structural frequency decreased, the Asym NES outperformed the other two control devices, having the lowest displacement RMSs under majority of the earthquakes considered. In conclusion, while the TMD was not suitable for structures with changed frequencies and the cubic NES was not suitable for excitations with wide-ranged energies, the Asym NES overcame those shortcomings and exhibited strong frequency-robustness and energy-robustness even under complex seismic excitations.

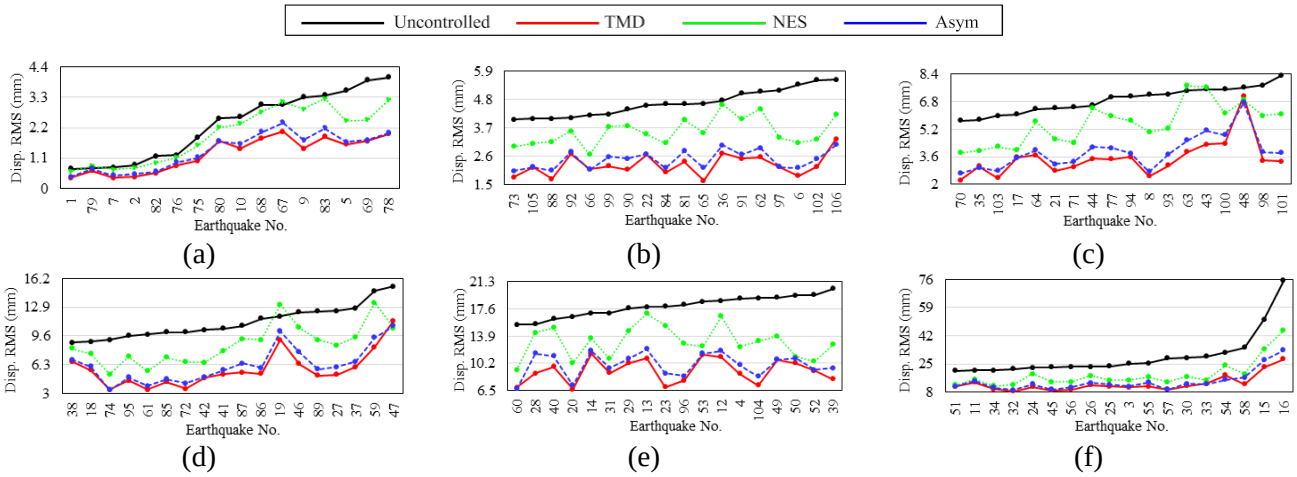

Fig. 7 – RMS top story displacements of original-frequency structures under seismic excitations: (a) 0 mm to 4.4 mm, (b) 1.5 mm to 5.9 mm, (c) 2 mm to 8.4 mm, (d) 3 mm to 16.2 mm, (e) 6.5 mm to 21.3 mm, and (f) 8 mm to 76 mm

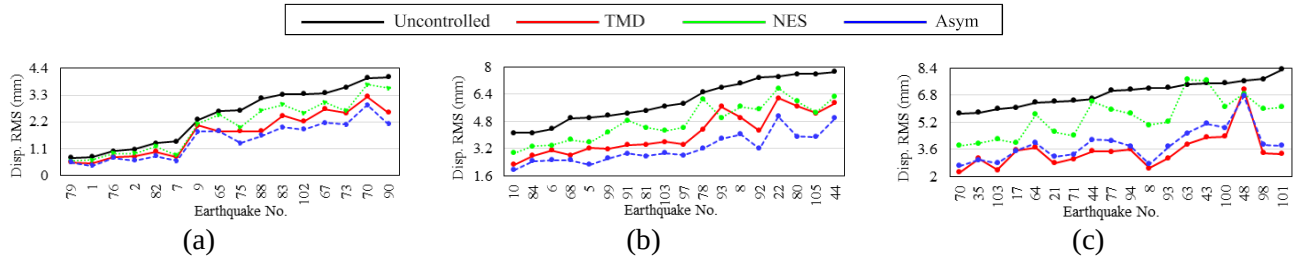

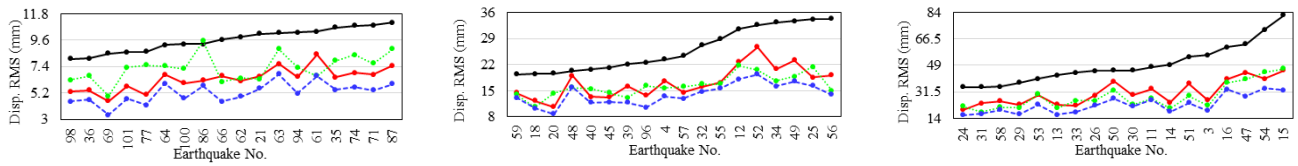

Fig. 8 – RMS top story displacements of decreased-frequency structures under seismic excitations: (a) 0 mm to 4.4 mm, (b) 1.6 mm to 8 mm, (c) 2 mm to 8.4 mm, (d) 3 mm to 11.8 mm, (e) 8 mm to 36 mm, and (f) 14 mm to 84 mm

5. Conclusions

Asym NESs as a type of novel passive mass dampers are proposed in this study. Asym NESs are configured based on cubic NESs and consist of two types of springs including a cubic spring and a linear spring. The Asym NES mass is pulled to a new reference position where the cubic and linear spring forces are statically balanced. The restoring force of the Asym NES and the EOMs of an Asym NES-attached structure were derived. The experiment was carried out to validate the analytical and numerical models of the Asym NES and the experimental responses were compared between the Asym NES and the comparable TMD and cubic NES. The validated numerical model was then applied to further investigate the performance of the Asym NES on a six-story benchmark building when subjected to 106 seismic ground motions as a more realistic example. The conclusions are drawn as follows:

1. The Asym NES has an asymmetric restoring force which exhibits both nonlinearity and linearity. The nonlinear component enables the Asym NES to resonate with a wide range of frequencies and the linear component can alleviate the performance sensitivity to input energy levels.

2. The experiment on the small-scale three-story steel frame structure showed that all the three devices performed very well on the six-column structure which they were originally designed for. The Asym NES and the cubic NES outperformed the detuned TMD on the four-column structure. The Asym NES showed frequency robustness which was as strong as the cubic NES.

3. The seismic analysis showed that Asym NES was as effective as the in-tune TMD regardless of the energy levels of the earthquakes. Besides, this effectiveness was not affected by the frequency decrease in the primary structure which might happen during earthquakes. The ingenious design and excellent efficiency of the Asym NES offer a promising control strategy of high-performance for structural response mitigation under extreme seismic events.

6. Acknowledgements

The authors are grateful for the financial support from the Natural Science Foundation of Hunan Province, China (Project No. 2018JJ3123), the National Natural Science Foundation of China (Project No. 51608190), and the Grand-in-Aid for Scientific Research (JSPS KAKENHI Grant No. JP 19F19077).

7. References

[1] Housner GW, Bergman LA, Caughey TK, Chassiakos AG, Claus RO, Masri SF, Skelton RE, Soong TT, Spencer BF, Yao JTP. Structural control: past, present, and future. *J Eng Mech* 1997;123(9):897-971.

[2] Li C, Li J, Qu Y. An optimum design methodology of active tuned mass damper for asymmetric structures. *Mech Syst Signal Process* 2010;24(3):746-765.

[3] Li C, Cao B. Hybrid active tuned mass dampers for structures under the ground acceleration. *Struct Contr Health Monit* 2015;22(4):757-773.

[4] Cao L, Li C. Enhanced hybrid active tuned mass dampers for structures. *Struct Contr Health Monit* 2018;25(2):e2067.

[5] Soong TT, Dargush GF. Passive energy dissipation systems in structural engineering. West Sussex: Wiley;1997.

[6] Sadek F, Mohraz B, Taylor AW, Chung RM. A method of estimating the parameters of tuned mass dampers for seismic applications. *Earth Eng Struct Dyn* 1997;26(6):617-635.

[7] Kwok KCS, Samali B. Performance of tuned mass dampers under wind loads. *Eng Struct* 1995;17(9):655-667.

[8] Ghorbani-Tanha AK, Noorzad A, Rahimian M. Mitigation of wind-induced motion of Milad Tower by tuned mass damper. *Struct Des Tall Spec 2009*;18(4):371-385.

[9] Lu X, Li P, Guo X, Shi W, Liu J. Vibration control using ATMD and site measurements on the Shanghai World Financial Center Tower. *Struct Des Tall Spec* 2014;23(2):105-123.

[10] Den Hartog JP. Mechanical vibrations, 4th edition. McGraw-Hill, New York;1956.

[11] Warburton GB. Optimum absorber parameters for various combinations of response and excitation parameters. *Earth Eng Struct Dyn* 1982;10(3):381-401.

[12] Tsai HC, Lin GC. Optimum tuned-mass dampers for minimizing steady-state response of support-excited and damped structures. *Earth Eng Struct Dyn* 1993;22(11):957-973.

[13] Bakre SV, Jangid RS. Optimum parameters of tuned mass damper for damped main system. *Struct Contr Health Monit* 2007;14(3):448-470.

[14] Miranda JC. Discussion of system intrinsic parameters of tuned mass dampers used for seismic response reduction: System Intrinsic Parameters of TMDs. *Struct Contr Health Monit* 2016;23:349-368.

[15] Lavan O. Multi-objective optimal design of tuned mass dampers. *Struct Contr Health Monit* 2017;24:e2008.

[16] Sladek JR, Klingner RE. Effect of tuned-mass dampers on seismic response. J *Struct Eng* 1983;109(8):2004-2009.

[17] Rana R, Soong TT. Parametric study and simplified design of tuned mass dampers. *Eng Struct* 1998;20(3):193-204.

[18] Soto-Brito R, Ruiz SE. Influence of ground motion intensity on the effectiveness of tuned mass dampers. *Earth Eng Struct Dyn* 1999; 28(11):1255-1271.

[19] Aubry S, Kopidakis G, Morgante AM, Tsironis GP. Analytic conditions for targeted energy transfer between nonlinear oscillators or discrete breathers. *Physica B* 2001;296(1-3), 222–236.

[20] Kopidakis G, Aubry S, Tsironis GP. Targeted energy transfer through discrete breathers in nonlinear systems. *Phys Rev Lett* 2001;87(16):165501.

[21] Vakakis AF, Gendelman OV. Energy pumping in nonlinear mechanical oscillators: part II—resonance capture. *J Appl Mech* 2001;68(1):42-48.

[22] Vaurigaud B, Ture Savadkoohi A, Lamarque CH. Targeted energy transfer with parallel nonlinear energy sinks. part I: design theory and numerical results. *Nonlinear Dyn* 2011;66(4):763–80.

[23] Savadkoohi AT, Vaurigaud B, Lamarque CH, Pernot S. Targeted energy transfer with parallel nonlinear energy sinks, part II: theory and experiments. *Nonlinear Dyn* 2012;67(1):37-46.

[24] McFarland DM, Kerschen G, Kowtko JJ, Lee YS, Bergman LA, Vakakis AF. Experimental investigation of targeted energy transfers in strongly and nonlinearly coupled oscillators. *J Acoust Soc Am* 2005;118(2):791-799.

[25] Hubbard S, Spencer J, B. F, Bergman LA, Fahnestock LA, Vakakis AF, Wierschem NE, et al. Experimental testing of a large 9-story structure equipped with multiple nonlinear energy sinks subjected to an impulsive loading. *Struct Congress* 2013;2241-2252.

[26] Wierschem NE, Luo J, AL-Shudeifat M, Quinn DD, McFarland DM, Vakakis AF, et al. Realization of a strongly nonlinear vibration-mitigation device using elastomeric bumpers. *J Eng Mech* 2014;140(5):4014009.

[27] Wang J, Wierschem N, Spencer BF, Lu X. Experimental study of track nonlinear energy sinks for dynamic response reduction. *Eng Struct* 2015;94:9-15.

[28] Wang J, Wierschem N, Spencer BF Jr, Lu X. Numerical and experimental study of the performance of a single-sided vibro-impact track nonlinear energy sink. *Earth Eng Struct Dyn* 2016;45(4):635-652.

[29] Wang J, Wierschem N, Wang B, Spencer BF Jr. Multi-objective design and performance investigation of a high-rise building with track nonlinear energy sinks. *Struct Des Tall Spec* 2019;29(2): e1692.

[30] Sapsis T, Quinn D, Vakakis A, Bergman L. Effective stiffening and damping enhancement of structures with strongly nonlinear local attachments. *J Vib Acoust -Transactions of the ASME* 2012; 134:11016.

[31] Wang J, Liu Z, Hao W, Liu F. Combined linear and nonlinear structural control strategies for seismic response mitigation, *13th International Workshop on Advanced Smart Materials and Smart Structures Technology*, Tokyo, Japan, July 22-23, 2017.

[32] Wang J, Wang B, Liu Z, Zhang C, Li H. Experimental and numerical studies of a novel asymmetric nonlinear mass damper for seismic response mitigation, *Struct Contr Health Monit* 2020; e2513.

[33] MATLAB R2014a, The MathWorks, Inc., Natick, Massachusetts, United States.

[34] FEMA P-751. 2009. NEHRP recommended seismic provisions: design examples. Federal Emergency Management Agency, Washington, DC; 2012.

[35] PEER NGA database. The Pacific Earthquake Engineering Research Center. http://ngawest2.berkeley.edu Pacific Earthquake Engineering Research Center (PEER); 2017.

